metals

MDPI

Article

Continuous Dynamic Recrystallization and Deformation Behavior of an AA1050 Aluminum Alloy during High-Temperature Compression

Qi Yang, Tomasz Wojcik and Ernst Kozeschnik *

Institute of Materials Science and Technology, TU Wien, Getreidemarkt 9, 1060 Vienna, Austria
* Correspondence: ernst.kozeschnik@tuwien.ac.at

Abstract: Continuous dynamic recrystallization (CDRX) forms a new recrystallized microstructure through the progressive increase in low-angle boundary misorientations (LAGBs) during the hot forming of metallic materials with high stacking fault energy (SFE), such as aluminum alloys. The present work investigates the effect of deformation parameters on the evolution of the dynamic recrystallization microstructures of an AA1050 aluminum alloy during compression at elevated temperatures. The alloy microstructure is investigated at deformation temperatures and strain rates in the range of 300 °C to 500 °C and 0.001 to 0.8 s^{-1}. A well-defined substructure and subsequent DRX grains provide indication that recrystallization can proceed with continued strain under high-temperature compression. At a strain rate of 0.1 s^{-1}, the DRX fraction is observed to be 0.25 at a temperature of 300 °C. This fraction increases to 0.32 as the temperature rises to 400 °C. The recrystallization mechanism is identified by analyzing the flow stress, the evolution of the subgrain misorientation angle, and the distribution of recrystallized grains. The observations of discontinuous dynamic recrystallization (DDRX) and CDRX under various deformation parameters are discussed. Moreover, the main substructure evolution laws observed from the high-temperature compression of an AA1050 Al alloy are summarized.

Keywords: dynamic recrystallization; microstructure; flow curve; high-temperature compression; aluminum alloy

check for updates

Citation: Yang, Q.; Wojcik, T.; Kozeschnik, E. Continuous Dynamic Recrystallization and Deformation Behavior of an AA1050 Aluminum Alloy during High-Temperature Compression. *Metals* **2024**, *14*, 889. https://doi.org/10.3390/met14080889

Academic Editor: Elena Pereloma

Received: 27 June 2024
Revised: 26 July 2024
Accepted: 2 August 2024
Published: 4 August 2024

Copyright: © 2024 by the authors. Licensee MDPI, Basel, Switzerland. This article is an open access article distributed under the terms and conditions of the Creative Commons Attribution (CC BY) license (https://creativecommons.org/licenses/by/4.0/).

1. Introduction

Aluminum alloys are widely used in automotive, aerospace, and other industries due to their lightweight properties and mechanical performance. Hot forming of aluminum alloys is a rather complex metallurgical process, including work hardening (WH), dynamic recovery (DRV), static recovery (SRV), dynamic recrystallization (DRX), grain growth, etc. [1–3] Over the past few decades, many researchers [4–6] have studied the recrystallization behavior and microstructure evolution of different materials. The recrystallization and related annealing phenomena largely determine the final microstructure and mechanical properties of the alloys.

For aluminum alloys, it is generally accepted that dynamic recovery is an essential softening mechanism during hot forming, which is attributed to their high-stacking fault energy. In addition, dynamic recrystallization may occur, as frequently observed with advanced experimental characterization techniques. The DRX mechanisms in Al alloys are classified into three types: discontinuous dynamic recrystallization (DDRX) [7–9], continuous dynamic recrystallization (CDRX) [10–13], and geometric dynamic recrystallization (GDRX) [14,15]. DDRX usually occurs in high-purity Al [16], in Al-Mg-Mn alloys with high Mg solute addition [17], and in aluminum alloys that contain large particles (>1 μm) [18]. DDRX is characterized by clearly distinguishable nucleation and growth stages. GDRX usually occurs when grains become highly elongated during large strain deformation, and the grain thickness approaches roughly one to two times the subgrain size. McQueen and

co-workers [14] observed GDRX in the large strain hot forming of aluminum alloys. Also, GDRX was found in aluminum alloys [19] during severe strain and hot deformation of Al-Mg-Si alloys [20].

In the hot forming process, CDRX is the most commonly occurring mechanism observed in Al alloys, having been observed in equal-channel angular extrusion of Al-Li-Mg-Sc alloys [11], hot compression of AA7075 [21], hot torsion of Al-Mg-Si alloys [22], hot deformation of aluminum alloy 7055 with strain rates $\leq 0.1\ s^{-1}$ [23], hot deformation of the 2195 aluminum alloy at high temperatures (420–520 °C) [24], and others. In contrast to DDRX, CDRX is a non-nucleation process; the mechanism of CDRX is the continuous rotation of subgrains [25,26]. The permanent absorption of new mobile dislocations into low-angle subgrain boundaries (LAGBs) increases their misorientation until the LAGBs finally transform into high-angle grain boundaries (HAGBs).

The question of whether dynamic recrystallization proceeds as continuous, discontinuous, or geometric dynamic recrystallization is largely controlled by the particular hot deformation conditions [27]. It is interesting to note that the occurrence and transition of recrystallization will change by variations in temperature or initial grain size, among other factors, even for the same material. For example, DDRX and CDRX are reported for high-SFE high-purity Al [28,29]. Zhang et al. [24] reported that DDRX is the main DRX mechanism at 300–360 °C and CDRX is the main mechanism at 420–520 °C for the 2195 Al alloy. Thus, exploring the microstructural evolution of Al alloys would play a crucial role in understanding such a phenomenon. In this study, an AA1050 pure aluminum alloy is selected due to its minimal solute atoms and precipitated particles, which act as tangled locations for dislocation structure generation in other aluminum series.

The present study investigates the effect of deformation parameters on the evolution of the dynamic recrystallization microstructures for an AA1050 aluminum alloy under thermal compression loading. The occurrence of a well-defined substructure and subsequent DRX grains can provide indications that recrystallization can proceed with continued strain under high-temperature compression. The microstructures are analyzed under different temperatures and strain rates, and different recrystallization mechanisms are evaluated by analyzing the flow stress, the variation in misorientation angles, and the distribution of recrystallized grains. The criteria for DDRX and CDRX under different deformation parameters are quantified using experimental data, leading to the determination of a maximum temperature window for recrystallization. In addition, the observations and mechanisms of DDRX and CDRX are discussed.

2. Materials and Methods

The material investigated in this research is an AA1050 aluminum alloy provided by Neuman Aluminium Austria GmbH (Neuman Aluminium, Marktl, AT). in the form of aluminum billets. The chemical composition is summarized in Table 1. The specimens were machined into cylinders from the center position of the billet, with a diameter of 5 mm and a height of 10 mm. To minimize friction between the specimen and the dies, the end faces of the specimens were polished. Graphite lubricant and a tantalum sheet were used between the surfaces of anvils and specimens.

Table 1. Chemical composition of AA1050 aluminum alloy (wt%).

Si	Fe	Cu	Mn	Mg	Cr	Zn	Ti	Al
0.08	0.26	<0.01	<0.01	<0.01	<0.01	<0.01	<0.01	99.63

Single-pass isothermal compression was performed on a high-speed quenching and deformation dilatometer, DIL 805 A/D, from Bähr. In the investigation, a temperature range from 300 °C to 500 °C and a strain rate range from 0.001 to 0.8 s^{-1} were used for thermo-mechanical processing and computer simulation. This corresponds to a deformation temperature range of $0.5\ T_m < T_{def} < 0.7\ T_m$, as recommended for CDRX by Sakai et al. [30] and Driver [31]. The melting temperature of the alloy is 625 °C, as calculated with

MatCalc [32] software version 6.04 (http://matcalc.at) and the open mc_al.tdb database (version 2.036) available on the MatCalc web site.

As shown in Figure 1, the specimens were heated to the deformation temperature at a heating rate of 10 K/s and held for 180 s before compression, followed by compression under different conditions. The true strain ranged from 0 to 0.9. To preserve the subgrain/grain structure and the occurrence of the DRX, the specimens were high-speed quenched with almost 100 K/s cooling speed to room temperature immediately after compression.

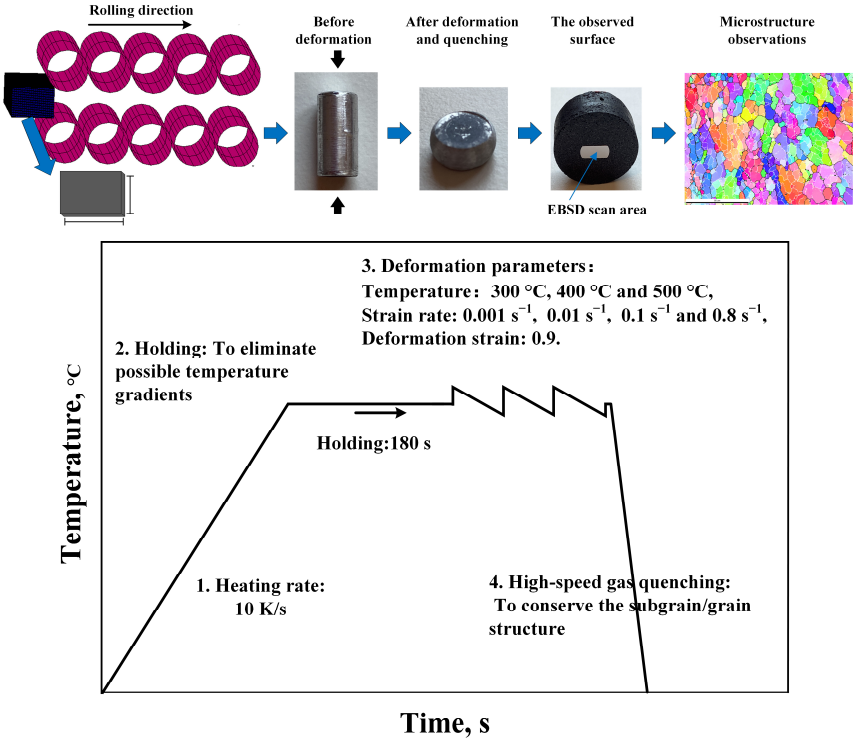


Figure 1. Schematic of the isothermal compression test procedures.

Electron backscatter diffraction (EBSD, EDAX Inc., Mahwah, NJ, USA) measurement was carried out using a Zeiss Sigma 500VP high-resolution scanning electron microscope with an EDAX detector (Zeiss, Oberkochen, DE). The sample preparation for EBSD consists of standard mechanical grinding and polishing, followed by OP-S polishing with an automatic polishing device (Struers Inc., Hovedstaden, DK). EBSD mappings were recorded at an accelerating voltage of 20 kV and a step size of 0.5 μm at the center of the deformed regions of the mid-width location. The data processing of EBSD results was completed by using EDAX OIM Analysis8 software (v8, EDAX Inc., Mahwah, NJ, USA).

3. Results

3.1. Microstructure Evolution

The microstructure evolution of the AA1050 aluminum alloy is characterized by electron backscatter diffraction (EBSD). Figure 2a–c show the microstructure after compression at temperatures of 300 °C, 400 °C, and 500 °C. The true strain in the experiments is 0.9. Low-angle subgrain boundaries (LAGBs) with 2° < misorientation < 15° and high-angle grain boundaries (HAGBs) with misorientation > 15° are shown as white and black lines, respectively. From the inverse pole figure (IPF) maps, a duplex grain structure is observed stemming from (I) deformed parent grains with elongated shapes perpendicular to the direction of compression; (II) the recovered microstructure with a large number of equiaxed LAGBs within the elongated parent grains due to DRV; (III) the recrystallized microstructure with a large number of newly formed fine grains within parent grains or near/on the

parent grain boundaries. A combination of (I), (II), and (III) leads to a typical microstructure comprising LAGBs and HAGBs.

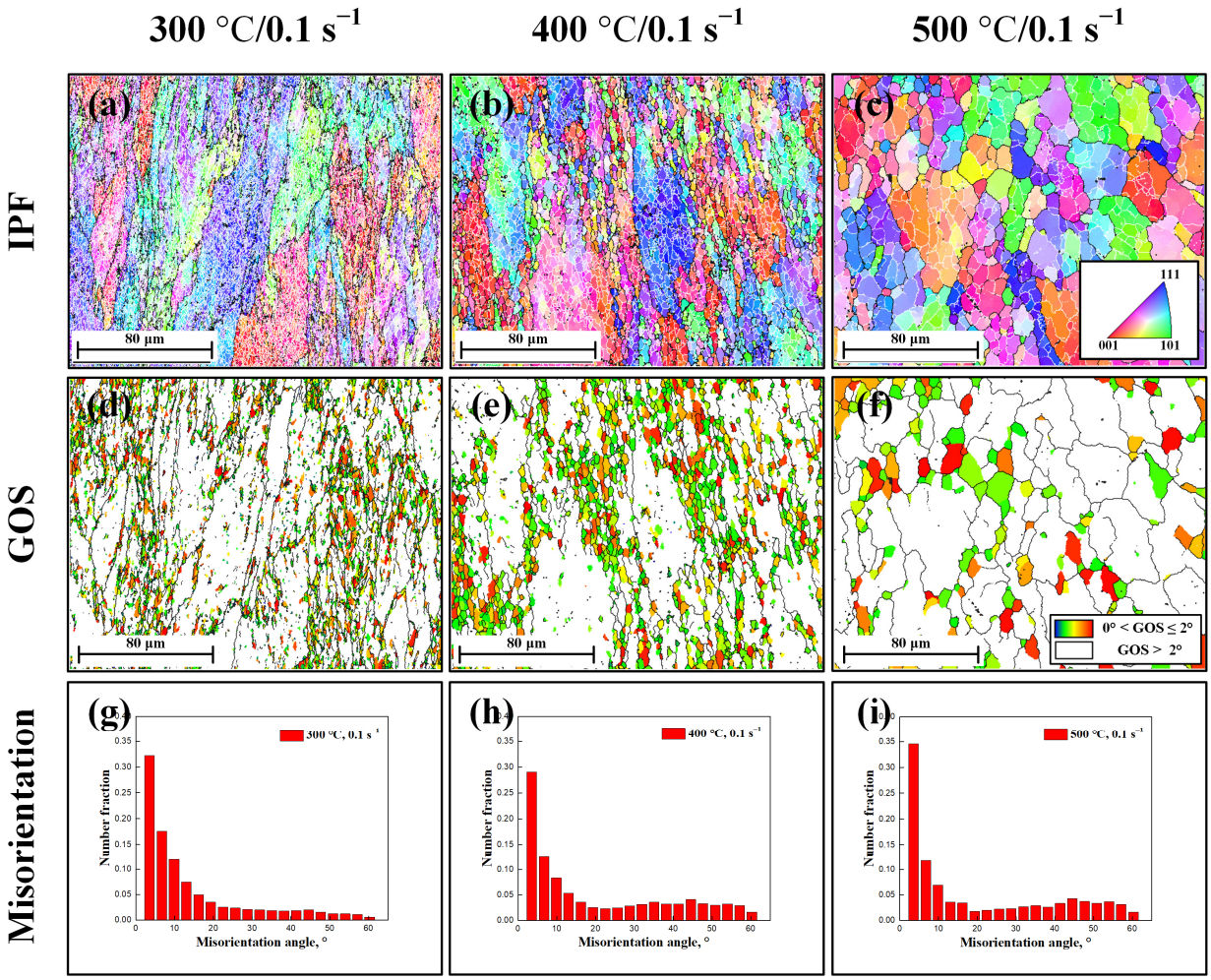


Figure 2. EBSD images of AA1050 aluminum alloy deformed to a strain of 0.9 with a strain rate of 0.1 s^{-1}: (**a**–**c**) inverse pole figure (IPF) maps of the specimens deformed at 300, 400, and 500 °C; (**d**–**f**) grain orientation spread (GOS) maps with high-angle grain boundaries; and (**g**–**i**) distribution histograms of misorientation angle.

Figure 2a shows the microstructure after deformation at 300 °C and a strain rate of 0.1 s^{-1}. The interior of the elongated grains contains a high density of LAGBs, which is the typical substructure observed after DRV. In materials with high SFE (such as Al, Ti, etc.), and in contrast to those with low and medium SFE (deformation conditions under which DRV is not particularly rapid), the rearrangement and annihilation of dislocations readily take place through DRV, leading to the formation of LAGBs in the pancaked parent grains [30,33]. Moreover, some fine recrystallized grains are visible within the deformed parent grains, although DRV (main softening type) reduces the driving force for the occurrence of DRX.

More recrystallized grains with equiaxed morphology are observed in Figure 2b,c. An increase in temperature promotes the generation of subgrain boundaries and their mobility, thus promoting the formation of DRX grains [30,33]. Obviously, the average size of subgrains increases with temperature. The average subgrain size of the specimens deformed to strain 0.9 at different deformation conditions of 300 °C/0.1 s^{-1}, 400 °C/0.1 s^{-1}, and 500 °C/0.1 s^{-1} is obtained as 1.70 μm, 3.50 μm, 11.00 μm, respectively. The effect of the strain rate on the microstructure is shown in Figure 3. Fine subgrains and recrystallized grains are generated at low strain rates, which emphasizes that the low strain rate promotes DRX at this temperature. The lower strain rate corresponds to an elongation of the defor-

mation time, which supports the transition from LAGBs to new DRX grain boundaries and, thus, the formation of DRX grains [34].

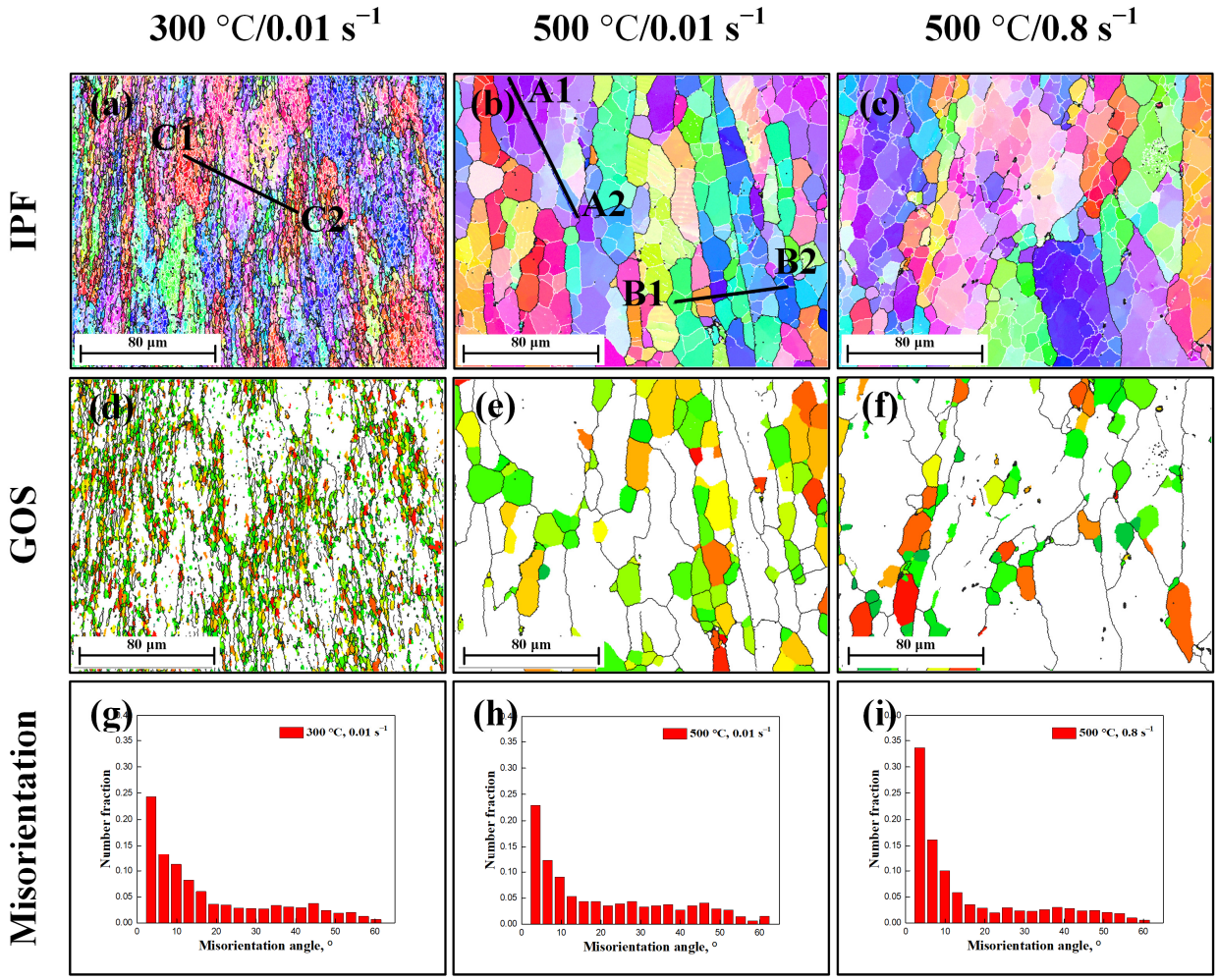


Figure 3. EBSD images of AA1050 aluminum alloy deformed to strain of 0.9: (**a**–**c**) IPF maps of specimens deformed at 300 °C/0.01 s^{-1}, 500 °C/0.01 s^{-1}, and 500 °C/0.8 s^{-1}; (**d**–**f**) GOS maps with high-angle grain boundaries; and (**g**–**i**) distribution histograms of misorientation angle.

The corresponding distribution histograms of misorientation angles are shown in Figures 2 and 3. It was clear that the misorientation angle exhibited a relatively random distribution. The average misorientation angle of the specimens gradually increased with increasing deformation temperature or decreasing strain rate. Accordingly, low-angle subgrain boundaries absorbing dislocations and transforming into HAGBs were responsible for an increase in the misorientation angle, which is also considered a typical identification of DRX phenomena [1,30,33].

The misorientation profiles along the black lines A1 to A2, B1 to B2, and C1 to C2 in Figure 3a,b are displayed in Figure 4, which represents the distribution of local point-to-point and cumulative (point-to-origin) misorientations developed in grain interiors along the lines. In the misorientation profile, several low misorientation fluctuations can be observed, which confirms the formation of new subgrains. More misorientation angles greater than 15° indicate the occurrence of subgrain rotation, accompanied by the formation of new recrystallized grains.

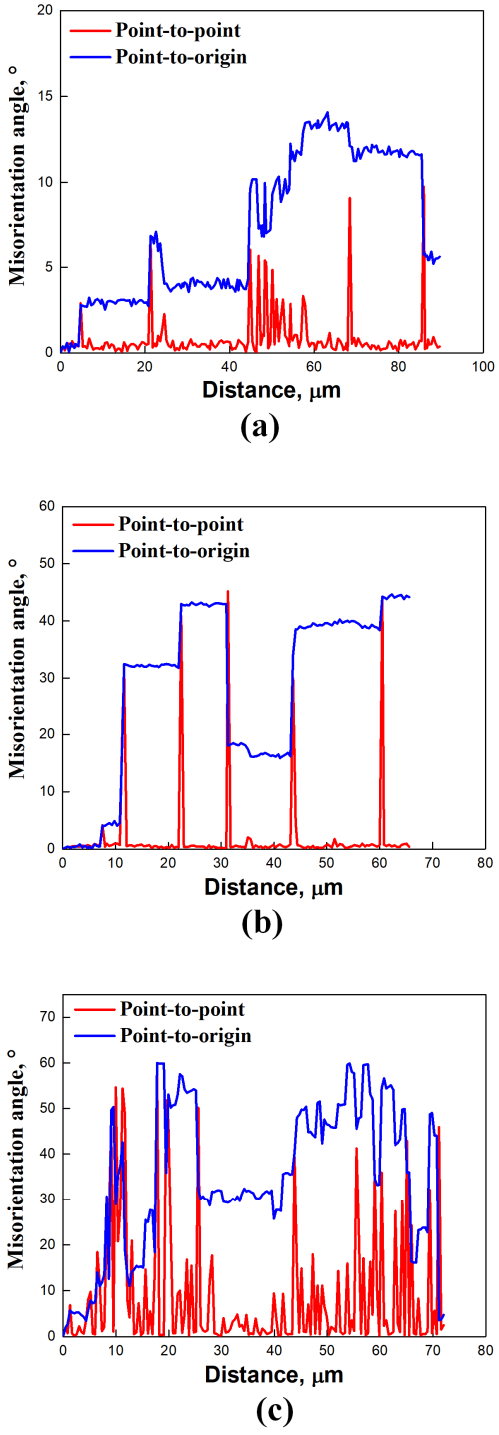


Figure 4. Cumulative misorientation profiles along the lines of recrystallized grains: (**a**) A1–A2, (**b**) B1–B2, and (**c**) C1–C2.

3.2. DRX at Medium or High Temperatures

The grain orientation spread (GOS) is used to assist in observing the characteristics of DRX, which denotes the deviation in the misorientation angles of every pixel of a grain with respect to the mean grain orientation. The grains with a GOS less than 2° are regarded as DRX grains.

Figures 2d and 3d show the GOS maps of the specimens deformed at 300 °C, in which two characteristics of DRX are observed. Partially recrystallized grains are mainly located along the grain boundary with a necklace structure, which is consistent with the result

that DDRX can occur at medium temperatures [24]. The corresponding grain boundary map of the specimens deformed at a medium temperature (300 °C) is shown in Figure 5a. Recrystallized grains that are nucleated directly inside the parent grains can also be found, demonstrating the existence of CDRX. Therefore, two types of recrystallization coexist at this temperature.

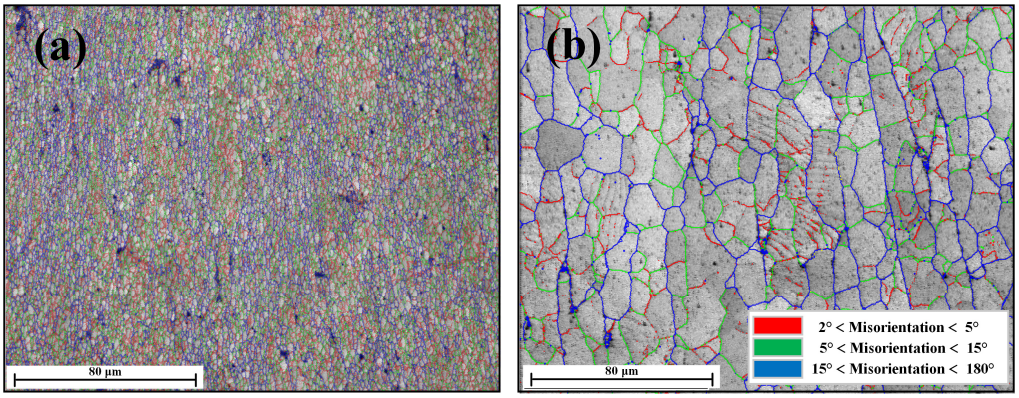


Figure 5. Grain boundary maps of the specimens deformed at (**a**) 300 °C/0.01 s^{-1} and (**b**) 500 °C/0.01 s^{-1} (red, green, and blue lines represent boundaries with misorientation angles in the 2–5°, 5–15°, and >15° ranges, respectively).

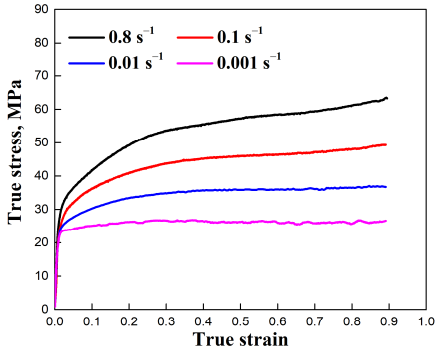
Through the GOS maps of Figure 2, an obtained conclusion is that the DRX fraction in the microstructure gradually increases with a decrease in the strain rate or an increase in temperature. When the strain rate is 0.1 s^{-1}, the DRX fraction at a temperature of 300 °C is observed to be 0.25. This fraction increases to 0.32 as the temperature rises to 400 °C, confirming the occurrence of recrystallization during deformation. Concurrently, the size of DRX grains shows visible increases with the elevation of the deformation temperature. At a deformation temperature of 500 °C, the DRX fraction at a strain rate of 0.01 s^{-1} is 0.34, representing a significant increase from 0.20 at a strain rate of 0.8 s^{-1} (see Figure 3).

When subjected to deformation at high temperatures, the presence of coarse subgrains becomes evident, as seen in Figure 5b. There is no obvious necklace structure, and the DRX process is constituted in the transformation from LAGBs to HAGBs.

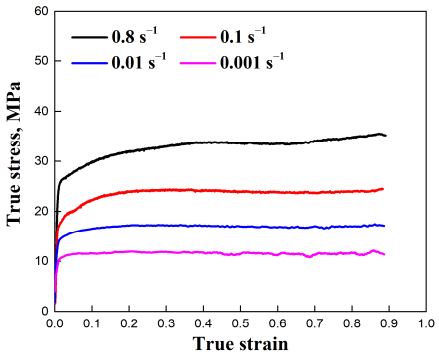
3.3. Flow Stress Behavior

The flow curves measured for various deformation parameters are shown in Figure 6. The true strain of deformation is between 0 and 0.9. At the early stage of deformation, work hardening plays the dominant role, leading to dislocation multiplication and tangling, resulting in a continuous increase in the flow stress. With continuing deformation, the dynamic softening mechanisms become increasingly prominent and eventually balance the continuous generation of dislocations. The dynamic softening effect can be exhibited by either dynamic recrystallization (DRX) and/or dynamic recovery (DRV), with both processes leading to either a plateau in the flow stress curve or even a reduction in stress. In the latter case, the flow stress curve is characterized by a peak. For Al alloys, both types of softening are observed [33]. As expected, the flow stress is sensitive to deformation temperature and strain rate, i.e., the flow stress decreases with an increasing deformation temperature or a decreasing strain rate.

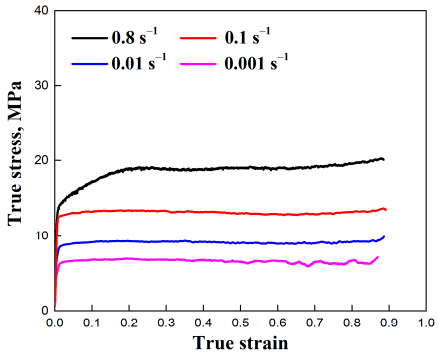
The critical strain associated with the initiation of DRX is a pivotal quantity in studies of material behavior with continuous deformation. According to Poliak and Jonas [35] and Ryan and McQueen [36], the characteristic strains of dynamic softening can be identified by analyzing the transition points on the θ–σ curve ($\theta = d\sigma/d\varepsilon$), where θ is the rate of work hardening (WH), σ is the true stress, and ε is the strain. The characteristic point curve in the flow curves is shown in Figure 7.



(a)



(b)



(c)

Figure 6. The stress–strain curves for various compression parameters: (**a**) 300 °C, (**b**) 400 °C, and (**c**) 500 °C.

First, the peak strain ε_p under different deformation conditions is evaluated from the experimental data of the AA1050 alloy and fitted with an Arrhenius-type equation as

$$\varepsilon_p = 0.00408\dot{\varepsilon}^{0.179}\left(\exp\left(\frac{142000}{RT}\right)\right)^{0.179}, \quad (1)$$

where $\dot{\varepsilon}$ is the strain rate, R is the gas constant, and T is the absolute deformation temperature. The value of deformation activation energy Q is 142 KJ.mol^{-1} for pure aluminum [37]. The relationship of lnε_p and ln ($\dot{\varepsilon}$exp (Q/RT) is plotted in Figure 8.

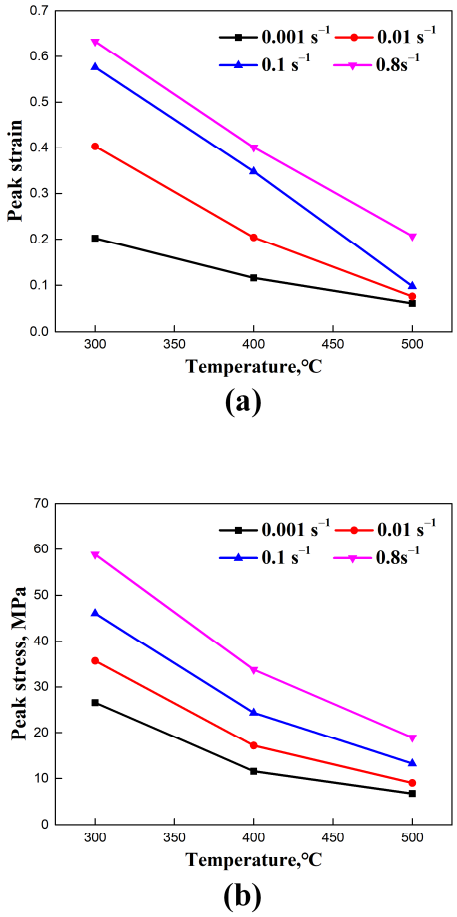


Figure 7. Characteristic point curves in the flow curves: (**a**) peak strain and (**b**) peak stress.

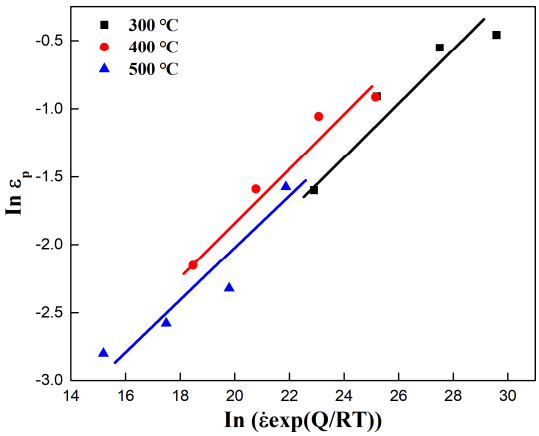


Figure 8. The relationship between ln ε_p and ln ($\dot{\varepsilon}$exp (Q/RT).

In previous reports [35,38], the easiest way to determine the critical strain ε_c for a given material is through the assumption of a critical strain ratio, which represents a fixed proportion between ε_c and ε_p. Accordingly, the calculation of the critical strain at which recrystallization initiates can be written as

$$\varepsilon_c = f_\varepsilon \varepsilon_p, \tag{2}$$

where f_ε is the critical strain ratio between critical strain and peak strain. For the determination of f_ε, the work of Cingara and McQueen [39] is utilized, where the value of f_ε is suggested to be in the order of 0.5.

4. Discussion

4.1. High-Temperature Deformation Behavior

It is well known that the complete thermal deformation process of most metals can be divided into four stages [1,40,41]: stage I (WH stage), stage II (transition stage), stage III (softening stage), and stage IV (steady-state stage). There have been many studies [1,30,33] describing these four stages in detail and the corresponding three typical behaviors of WH, DRV, and DRX.

Figure 9 illustrates the typical flow curves associated with various modes of dynamic softening, which result in different flow curve behaviors and their corresponding characteristics. For Al alloys (high SFE), two distinct forms of flow curves are typically observed, as illustrated in Figure 6. In the case of CDRX, competition between WH and dynamic softening (DRV and DRX) takes place, which slows down the increase rate of the flow stress. The microstructures displayed in Figures 2 and 3 clearly show that the softening is caused by DRV and DRX, resulting in the occurrence of a well-defined substructure and new fine recrystallized grains. The second type of high-temperature behavior is characterized by a continuous increase in flow stresses (mainly WH+DRV). The rate of strain hardening slowly decreases with deformation and approaches zero at high strains.

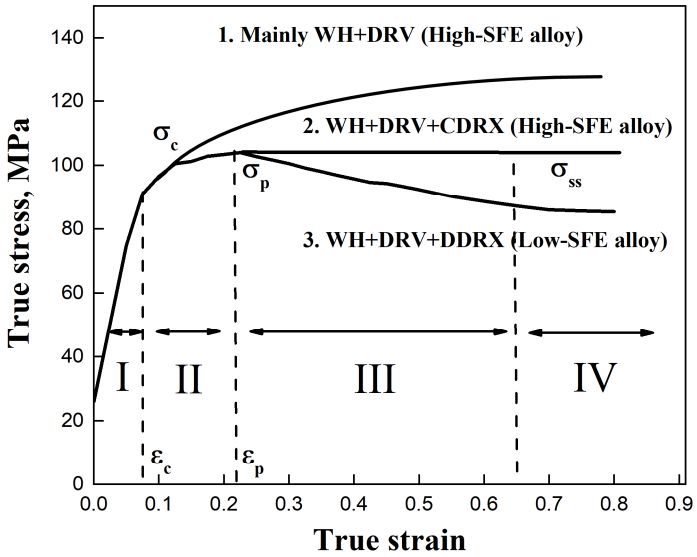


Figure 9. Typical flow curves for different modes of dynamic softening [1,30,33].

For Al alloys, the flow curves typically exhibit rapid stress saturation at high temperatures (case 2 in Figure 9), compared with the flow curve of DDRX. In addition, a continuously increasing flow curve (case 1 in Figure 9) can be found at a medium temperature (300 °C) and high strain rate. Figure 10 illustrates the microstructure obtained at 300 °C, a strain rate of 0.8 s^{-1}, and a strain of 0.9. Due to the high SFE, the operation of multiple slip systems leads to the formation of dense dislocation walls (DDWs) on the slip planes [42]. A substantial increase in fine substructures results in a higher dislocation density of geometrically necessary boundaries (GNBs), thereby resulting in a continued increase in flow stress. The microstructures presented in Figures 2 and 3 demonstrate a significant influence of temperature and strain rate on the substructure. The formation of finer subgrains is observed at a temperature of 300 °C (almost 0.5 T_m) and a high strain rate, in accordance with the conclusions reported by Yang et al. [43]. The formation of a cell-like substructure and dislocation strengthening contribute to a sustained upward trend in the flow curve of hot deformation.

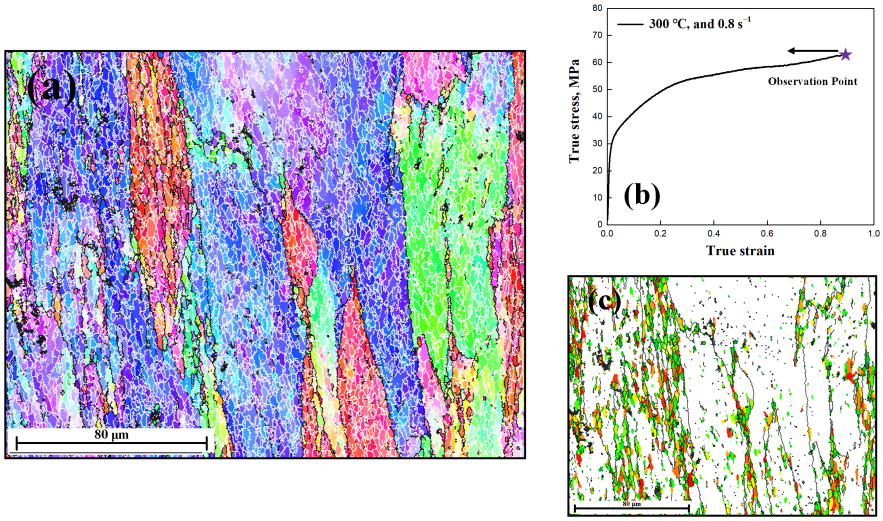


Figure 10. (**a**) Microstructure obtained at 300 °C/0.8 s^{-1}, with strain of 0.9; (**b**) corresponding flow curve; and (**c**) corresponding GOS map.

4.2. DDRX to CDRX Accompanied by Temperature and Strain Rate Changes

The detailed recrystallization grain boundary characteristics are shown in Figure 11. A more detailed EBSD observation is employed to investigate the evolution of subgrain and DRX boundaries (the scale is 20 microns in maps). As shown in Figure 11a, the substructure is formed with insufficient thermal energy to exhibit strong DRV [44], thus making it difficult to form a polygonal structure. Therefore, DDRX leads to the formation of a necklace microstructure along the grain boundaries. Simultaneously, some already formed subgrains can still transform their LAGBs into HAGBs and form fine continuously recrystallized grains. So, two recrystallization modes persist simultaneously at this temperature.

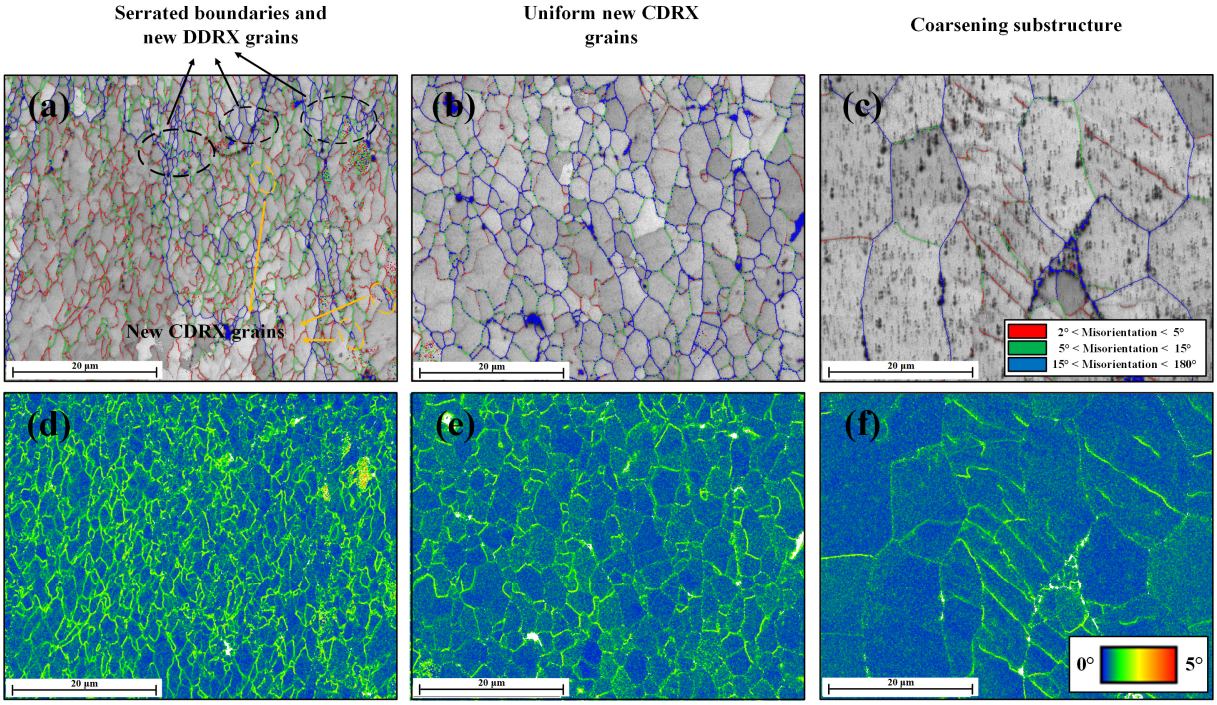


Figure 11. EBSD images of an AA1050 aluminum alloy deformed at different temperatures to a strain of 0.9: (**a**–**c**) grain boundary maps of the specimens deformed at (**a**) 300 °C/0.1 s^{-1}, (**b**) 400 °C/0.1 s^{-1}, and (**c**) 500 °C/0.1 s^{-1}; (**d**–**f**) corresponding KAM (Kernel Average Misorientation) maps.

Different from Figure 11a, more recrystallized grain boundaries are observed with increasing temperature, indicating more completed DRX (Figure 11b,c). Typical structures of DDRX, such as necklace structures and grain boundary bulging, do not appear. Instead, an equiaxed morphology is observed. This indicates that the nucleation mode of CDRX is mainly the formation of LAGBs by DRV, first, and the following transformation of LAGBs into HAGBs by subgrain rotation. It is also obvious from Figure 11b that the new recrystallized grains are uniformly distributed. As the temperature continues to increase, a coarser substructure is formed by the new grains, making the formation of new LAGBs difficult.

The KAM (Kernel Average Misorientation) maps support further discussion of results. Figure 11d shows the KAM map after deformation at 300 °C. The KAM adopts a higher value at LAGBs/grain boundaries, while a low KAM is observed in the grain interior. Higher KAM values refer to larger dislocation density and also higher stored deformation energy. Since dislocation generation continues while deformation proceeds, more and more dislocations are piled up to form new subgrains/LAGBs. Similarly, clear substructures visualized by high KAM stripes are also observed at higher temperatures (see Figure 11e,f). Gao et al. [45] report that the density of geometrically necessary dislocations (GNDs) is related to the local misorientation angle (KAM value) with $\rho_{GND} = 2\theta/\mu b$. If the average KAM increases sharply, the density of GNDs formed locally increases continuously.

Figure 12 shows the EBSD images after deformation at 300 °C and a low strain rate of 0.001 s^{-1}. It is worth noticing that the operation of various DRX modes is contingent upon the different strain rates. At a low strain rate of 0.001 s^{-1}, typical structures of DDRX, such as necklace structures and grain boundary bulging, are notably absent. The appearance of a well-defined substructure and incomplete HAGBs confirms the progressive transformation of subgrain boundaries towards recrystallized grain boundaries. This provides an indication for the operation of CDRX under these conditions. DDRX may occur but is not dominant. In contrast to the low strain rate, there is an acceleration in the migration of grain boundaries (HAGBs) at a higher strain rate, thus forming wavy shapes with different curvatures [46]. The extra driving force exerted along the parent grain boundaries leads to the bulging of these boundaries, thereby facilitating DDRX.

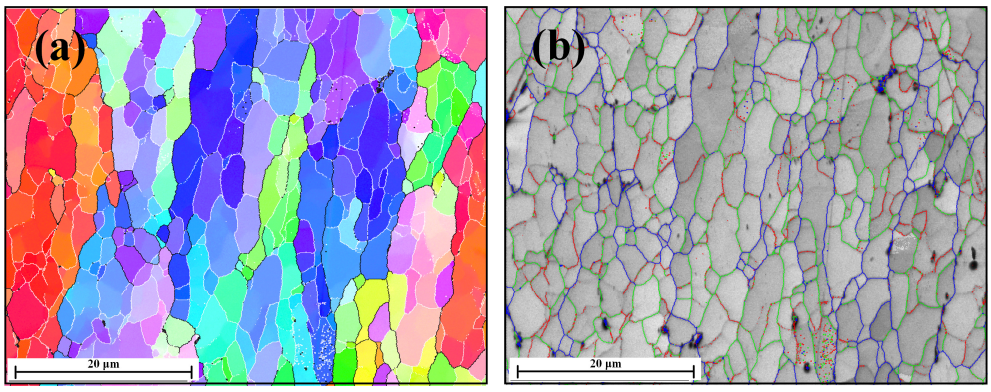


Figure 12. EBSD images of AA1050 aluminum alloy deformed (strain of 0.9) at 500 °C/0.001 s^{-1}: (**a**) IPF map and (**b**) corresponding grain boundary map.

4.3. Illustration of DRX Mechanisms

Figure 13 illustrates a sketch of the observed DRX mechanisms. Before deformation, the parent grains exhibit an initial microstructure with a relatively low excess dislocation density. Figure 13b describes the early stage of deformation, where dislocation accumulation through DRV leads to the formation of new subgrain boundaries, thereby inducing a significant reduction in the mean subgrain size. Subsequently, as deformation progresses, DRX starts to occur with the generation of new recrystallized grains and a concurrent decrease in overall dislocation density. Then, DRX and recovery processes persist until a steady state is eventually reached. On comparing Figures 2, 3 and 11, it is obvious that an

increase in temperature results in the formation of coarsening substructures. Additionally, there are notable changes in the types of DRX observed.

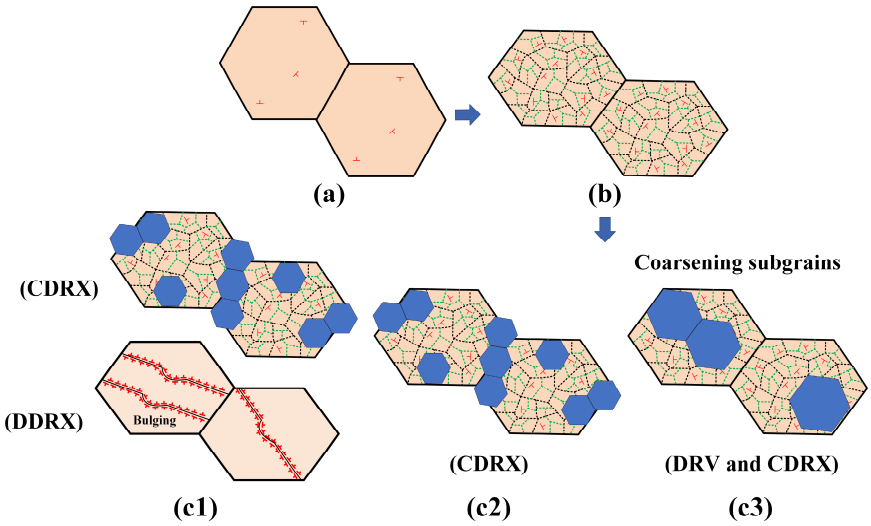


Figure 13. Schematic diagram of DRX mechanism: (**a**) initial microstructure before deformation, (**b**) generation of cells and subgrains, (**c1**) generation of recrystallized grains when the deformation temperature is almost 0.5 T_m, (**c2**) 0.5 T_m < deformation temperature < 0.7 T_m, and (**c3**) deformation temperature > 0.7 T_m.

Figure 13(c1) represents the coexistence of DDRX and CDRX at a deformation temperature of almost 0.5 T_m. For DDRX, the newly formed recrystallized grains exhibit a necklace-like structure as they nucleate and grow into areas characterized by a high dislocation density. This process is facilitated by the mechanism of grain boundary bulging when the stored energy is sufficient to start recrystallization [30,33]. The microstructures presented in Section 3 clearly demonstrate the transformation of LAGBs into HAGBs at high temperatures, which is characterized by a homogeneous increase in misorientation. New CDRX recrystallized grains are generated when the misorientation angles reach a critical value, in accordance with the conclusions reported by Huang et al. [33]. Figure 13(c2,c3) describe the recrystallization mechanism at high-temperature deformation with temperatures > 0.5 T_m, where CDRX is the main DRX mode.

The microstructure evolution and related discussion describe the formation of a well-defined substructure and subsequent DRX. The main substructure evolution laws observed from the high-temperature deformation of an AA1050 Al alloy can be summarized as follows: (i) The flow stress increases with strain, showing two different curve types for an AA1050 Al alloy. Similarly, the density of geometrically necessary dislocations (GNDs) increases with strain, accompanied by the formation of subgrain boundaries. The density of GNDs is greatly related to the subgrain size. (ii) The average subgrain size decreases with deformation. Additionally, the subgrain size is notably influenced by variations in deformation conditions. The present results show that the average subgrain size eventually reaches a "saturation value" at large strains, which is no longer sensitive to the strain [33,47,48]. (iii) DRX can occur during medium- or high-temperature compression of an AA1050 Al alloy, appearing as DDRX and/or CDRX, which is influenced by the deformation temperature, strain rate, strain, etc.

5. Conclusions

The hot deformation behavior, microstructure evolution, and the DRX mechanisms of an AA1050 aluminum alloy are investigated by high-temperature compression at various deformation parameters. The main conclusions are as follows:

(1) The typical effects of deformation conditions on the flow behavior of an AA1050 aluminum alloy are observed, revealing distinct variations in the flow curves associated

with recrystallization and recovery processes. The peak strain and critical strain under different deformation conditions are evaluated from the experimental data.

(2) A detailed DRX analysis is provided with subgrain/grain boundary characteristics. The formation of a well-defined substructure and the subsequent transformation of LAGBs to HAGBs are significant, which provides indication that recrystallization can proceed with continued strain under high-temperature compression. The DRX fraction at a condition of 300 °C/0.1 s^{-1} is observed to be 0.25. This fraction increases to 0.32 as the temperature rises to 400 °C. These deformation conditions have a clear effect on the microstructure, DRX fraction, and misorientation.

(3) The DRX process of the AA1050 aluminum alloy consists of DDRX and CDRX. The nucleation of DDRX grains occurs at the initial grain boundaries and is characterized by bulging of the initial high-angle grain boundaries. The second observed recrystallization type is the formation of fine recrystallized grains that occur inside the grains, which are considered to stem from CDRX. The mechanism and deformation parameters, in which recrystallization occurs, are discussed in detail in light of the experimental results.

(4) The occurrence of DDRX or CDRX varies with changes in deformation conditions, such as the temperature and strain rate. The coexistence of DDRX and CDRX at almost 0.5 T_m and a low strain rate has been observed, while CDRX is the main recrystallization mode when the deformation temperature is increased (>0.5 T_m). These variations determine the evolution of the substructure.

Author Contributions: Conceptualization, Q.Y. and E.K.; methodology, Q.Y., T.W. and E.K.; validation, Q.Y. and E.K.; formal analysis, Q.Y.; investigation, Q.Y. and T.W.; resources, E.K. and T.W.; data curation, Q.Y. and T.W.; writing—original draft preparation, Q.Y. and E.K.; writing—review and editing, E.K.; visualization, Q.Y., T.W. and E.K.; supervision, E.K.; project administration, E.K.; funding acquisition, Q.Y. and E.K. All authors have read and agreed to the published version of the manuscript.

Funding: This research received no external funding.

Data Availability Statement: The raw data supporting the conclusions of this article will be made available by the authors on request.

Acknowledgments: Open Access Funding by TU Wien. Qi Yang appreciates the financial support from the State Scholarship Fund of China (No. 202107710006) during his PhD at TU Wien.

Conflicts of Interest: The authors declare no conflicts of interest.

References

1. Humphreys, F.J.; Hatherly, M. *Recrystallization and Related Annealing Phenomena*, 2nd ed.; Elsevier: Oxford, UK, 2004.
2. Doherty, R.D.; Hughes, D.A.; Humphreys, F.J.; Jonas, J.J.; Jensen, D.J.; Kassner, M.E.; McNelley, T.R.; McQueen, H.J.; Rollet, A.D. Current issues in recrystallization: A review. *Mater. Sci. Eng. A* **1997**, *238*, 219–274. [CrossRef]
3. Lv, J.X.; Zheng, J.H.; Yardley, V.A.; Shi, Z.S.; Lin, J.G. A Review of Microstructural Evolution and Modelling of Aluminium Alloys under Hot Forming Conditions. *Metals* **2020**, *10*, 1516. [CrossRef]
4. Mirzadeh, H. Grain refinement of magnesium alloys by dynamic recrystallization (DRX): A review. *J. Mater. Res. Technol.* **2023**, *25*, 7050–7077. [CrossRef]
5. Zhang, H.K.; Xiao, H.; Fang, X.W.; Zhang, Q.; Logé, R.E.; Huang, K. A critical assessment of experimental investigation of dynamic recrystallization of metallic materials. *Mater. Des.* **2020**, *193*, 108873. [CrossRef]
6. Sakai, T.; Jonas, J.J. Dynamic recrystallization: Mechanical and microstructural considerations. *Acta Metall.* **1984**, *32*, 189–209. [CrossRef]
7. Son, H.W.; Lee, J.C.; Cho, C.H.; Hyun, S.K. Effect of Mg content on the dislocation characteristics and discontinuous dynamic recrystallization during the hot deformation of Al-Mg alloy. *J. Alloys Compd.* **2021**, *887*, 161397. [CrossRef]
8. Li, H.; Huang, Y.C.; Liu, Y. Dynamic recrystallization mechanisms of as-forged Al–Zn–Mg-(Cu) aluminum alloy during hot compression deformation. *Mater. Sci. Eng. A* **2023**, *878*, 145236. [CrossRef]
9. Ponge, D.; Bredehöft, M.; Gottstein, G. Dynamic recrystallization in high purity aluminum. *Scr. Mater.* **1997**, *37*, 1769–1775. [CrossRef]
10. Gourdet, S.; Montheillet, F. An experimental study of the recrystallization mechanism during hot deformation of aluminium. *Mater. Sci. Eng. A* **2000**, *283*, 274–288. [CrossRef]

11. Kaibyshev, R.; Shipilova, K.; Musin, F.; Motohashi, Y. Continuous dynamic recrystallization in an Al-Li-Mg-Sc alloy during equal-channel angular extrusion. *Mater. Sci. Eng. A* **2005**, *396*, 341–351. [CrossRef]
12. Sakai, T.; Miura, H.; Goloborodko, A.; Sitdikov, O. Continuous dynamic recrystallization during the transient severe deformation of aluminum alloy 7475. *Acta Mater.* **2009**, *57*, 153–162. [CrossRef]
13. Miao, J.S.; Sutton, S.; Luo, A.A. Deformation microstructure and thermomechanical processing maps of homogenized AA2070 aluminum alloy. *Mater. Sci. Eng. A* **2022**, *834*, 142619. [CrossRef]
14. McQueen, H.J.; Knustad, O.; Ryum, N.; Solberg, J.K. Microstructural evolution in Al deformed to strains of 60 at 400 °C. *Scr. Mater.* **1985**, *19*, 73–78. [CrossRef]
15. Blum, W.; Zhu, Q.; Merkel, R.; McQueen, H.J. Geometric dynamic recrystallization in hot torsion of Al-5Mg-0.6Mn (AA5083). *Mater. Sci. Eng. A* **1996**, *205*, 23–30. [CrossRef]
16. Chovet, C.; Gourdet, S.; Montheillet, F. Modelling the transition from discontinuous to continuous dynamic recrystallization with decreasing purity in aluminium. *Mater. Trans. JIM* **2000**, *41*, 109–112. [CrossRef]
17. Yang, B.; Gao, M.; Wang, Y.; Guan, R. Dynamic recrystallization behavior and mechanical properties response of rheo-extruded Al-Mg alloys with various Mg contents. *Mater. Sci. Eng. A* **2022**, *849*, 143450. [CrossRef]
18. Jazaeri, H.; Humphreys, F.J. The transition from discontinuous to continuous recrystallization in some aluminium alloys: I-the deformed state. *Acta Mater.* **2004**, *52*, 3239–3250. [CrossRef]
19. Henshall, G.A.; Kassner, M.E.; McQueen, H.J. Dynamic restoration mechanisms in Al-5.8 At. Pct Mg deformed to large strains in the solute drag regime. *Metall. Trans. A* **1992**, *23*, 881–889. [CrossRef]
20. Li, J.C.; Wu, X.D.; Cao, L.F.; Wang, Y.C.; Liu, Q. Hot deformation and dynamic recrystallization in Al-Mg-Si alloy. *Mater. Charact.* **2021**, *173*, 110976. [CrossRef]
21. Rokni, M.R.; Zarei-Hanzaki, A.; Roostaei, A.A.; Abedi, H.R. An investigation into the hot deformation characteristics of 7075 aluminum alloy. *Mater. Des.* **2011**, *32*, 2339–2344. [CrossRef]
22. Lee, J.W.; Son, K.T.; Jung, T.K.; Yoon, Y.O.; Kim, S.K.; Choi, H.J.; Hyun, S.K. Continuous dynamic recrystallization behavior and kinetics of Al-Mg-Si alloy modified with CaO-added Mg. *Mater. Sci. Eng. A* **2016**, *673*, 648–659. [CrossRef]
23. Liao, B.; Wu, X.D.; Cao, L.F.; Huang, G.J.; Wang, Z.A.; Liu, Q. The microstructural evolution of aluminum alloy 7055 manufactured by hot thermo-mechanical process. *J. Alloys Compd.* **2019**, *796*, 103–110. [CrossRef]
24. Zhang, J.J.; Yi, Y.P.; Huang, S.Q.; Mao, X.C.; He, H.L.; Tang, J.G.; Guo, W.F.; Dong, F. Dynamic recrystallization mechanisms of 2195 aluminum alloy during medium/high temperature compression deformation. *Mater. Sci. Eng. A* **2021**, *804*, 140650. [CrossRef]
25. Kaibyshev, R.; Malopheyev, S. Mechanisms of dynamic recrystallization in aluminum alloys. *Mater. Sci. Forum* **2014**, *794*, 784–789. [CrossRef]
26. Canelo-Yubero, D.; Kovács, Z.; Fotso, J.F.T.S.; Tolnai, D.; Schell, N.; Groma, I.; Poletti, C. In-situ characterization of continuous dynamic recrystallization during hot torsion of an Al-Si-Mg alloy. *J. Alloys Compd.* **2020**, *822*, 153282. [CrossRef]
27. Li, Q.; Ning, J.; Chen, L.; Hu, J.; Liu, Y. The mechanical response and microstructural evolution of 2195 Al–Li alloy during hot tensile deformation. *J. Alloys Compd.* **2020**, *848*, 156515. [CrossRef]
28. Yamagata, H.; Ohuchida, Y.; Saito, N.; Otsuka, M. Nucleation of new grains during discontinuous dynamic recrystallization of 99.998 mass% Aluminum at 453K. *Scr. Mater.* **2001**, *45*, 1055–1061. [CrossRef]
29. Sheppard, T.; Tutcher, M.G. Development of duplex deformation substructure during extrusion of a commercial Al-5Mg-0.8Mn alloy. *Met. Sci.* **1980**, *14*, 579–590. [CrossRef]
30. Sakai, T.; Belyakov, A.; Kaibyshev, R.; Miura, H.; Jonas, J.J. Dynamic and post-dynamic recrystallization under hot, cold and severe plastic deformation conditions. *Prog. Mater. Sci.* **2014**, *60*, 130–207. [CrossRef]
31. Driver, J. The limitations of continuous dynamic recrystallization (CDRX) of aluminium alloys. *Mater. Lett.* **2018**, *222*, 135–137. [CrossRef]
32. Kozeschnik, E. *Encyclopedia of Materials: Metals and Alloys*; Elsevier: Oxford, UK, 2022; Volume 4, pp. 521–526.
33. Huang, K.; Logé, R.E. A review of dynamic recrystallization phenomena in metallic materials. *Mater. Design* **2016**, *111*, 548–574. [CrossRef]
34. Zhang, H.; Zhang, K.; Zhou, H.; Lu, Z.; Zhao, C.; Yang, X. Effect of strain rate on microstructure evolution of a nickel-based superalloy during hot deformation. *Mater. Des.* **2015**, *80*, 51–62. [CrossRef]
35. Poliak, E.I.; Jonas, J.J. Critical strain for dynamic recrystallization in variable strain rate hot deformation. *ISIJ Int.* **2003**, *43*, 692–700. [CrossRef]
36. Ryan, N.D.; McQueen, H.J. Dynamic softening mechanisms in 304 austenitic stainless steel. *Can. Metall. Q.* **1990**, *29*, 147–162. [CrossRef]
37. Sherby, O.D.; Klundt, R.H.; Miller, A.K. Flow stress, subgrain size, and subgrain stability at elevated temperature. *Metall. Trans. A* **1977**, *8*, 843–850. [CrossRef]
38. Poliak, E.I.; Jonas, J.J. A one-parameter approach to determining the critical conditions for the initiation of dynamic recrystallization. *Acta Mater.* **1996**, *44*, 127–136. [CrossRef]
39. Cingara, A.; McQueen, H.J. New formula for calculating flow curves from high temperature constitutive data for 300 austenitic steels. *J. Mater. Process. Technol.* **1992**, *36*, 31–42. [CrossRef]
40. Smallman, R.E.; Bishop, R.J. *Modern Physical Metallurgy and Materials Engineering*; Butterworth-Heinemann: Oxford, UK, 1999.

41. Lin, Y.C.; Chen, M.S.; Zhong, J. Prediction of 42CrMo steel flow stress at high temperature and strain rate. *Mech. Res. Commun.* **2008**, *35*, 142–150. [CrossRef]
42. Zaefferer, S.; Baudin, T.; Penelle, R. A study on the formation mechanisms of the cube recrystallization texture in cold rolled Fe-36% Ni alloys. *Acta Mater.* **2001**, *49*, 1105–1122. [CrossRef]
43. Yang, Q.Y.; Deng, Z.H.; Zhang, Z.Q.; Liu, Q.; Jia, Z.H.; Huang, G.J. Effects of strain rate on flow stress behavior and dynamic recrystallization mechanism of Al-Zn-Mg-Cu aluminum alloy during hot deformation. *Mater. Sci. Eng. A* **2016**, *662*, 204–213. [CrossRef]
44. Zhang, C.S.; Liu, M.F.; Meng, Z.J.; Zhang, Q.Y.; Zhao, G.Q.; Chen, L.; Zhang, H.; Wang, J. Microstructure evolution and precipitation characteristics of spray-formed and subsequently extruded 2195 Al-Li alloy plate during solution and aging process. *J. Mater. Process. Technol.* **2020**, *283*, 116718. [CrossRef]
45. Gao, H.; Huang, Y.; Nix, W.D.; Hutchinson, J.W. Mechanism based strain gradient plasticity I. Theory. *J. Mech. Phys. Solids* **1999**, *47*, 1239–1263. [CrossRef]
46. Zhang, Y.; Godfrey, A.; Jensen, D.J. Local boundary migration during recrystallization in pure aluminium. *Scr. Mater.* **2011**, *64*, 331–334. [CrossRef]
47. Poletti, C.; Rodriguez-Hortalá, M.; Hauser, M.; Sommitsch, C. Microstructure development in hot deformed AA6082. *Mater. Sci. Eng. A* **2011**, *528*, 2423–2430. [CrossRef]
48. Sellars, C.M.; Zhu, Q. Microstructural modelling of aluminium alloys during thermomechanical processing. *Mater. Sci. Eng. A* **2000**, *280*, 1–7. [CrossRef]

Disclaimer/Publisher's Note: The statements, opinions and data contained in all publications are solely those of the individual author(s) and contributor(s) and not of MDPI and/or the editor(s). MDPI and/or the editor(s) disclaim responsibility for any injury to people or property resulting from any ideas, methods, instructions or products referred to in the content.